EVOLUTION OF NUCLEAR SHAPES AND EXOTIC DECAYS NEAR ^{56}Ni*

D. Rudolph, C. Andreoiu, J. Ekman, C. Fahlander

Department of Physics, Lund University, S-22100 Lund, Sweden

A. Gadea

Laboratori Nazionali di Legnaro, I-35020 Legnaro, Italy

and D.G. Sarantites

Chemistry Department, Washington University, St. Louis, MO 63130, USA

(Received November 2, 2000)

An overview of recent high-spin nuclear structure studies in proton-rich nuclides near the doubly-magic isotope ^{56}Ni is presented.

PACS numbers: 21.10.–k, 23.20.–g, 23.50.+z, 27.40.+z

1. Introduction

The recent advent of efficient 4π Germanium detector arrays such as Euroball [1] and Gammasphere [2] is providing a wealth of exciting and unexpected results in nuclear structure physics [3]. At many occasions the Germanium arrays are coupled to modern ancillary detector systems. These aim, for example, at the detection of the light particles, which are emitted in the course of fusion-evaporation reactions, and/or employ recoil separators to detect the prompt γ-radiation in coincidence with one of the recoiling nuclei.

Such powerful combinations significantly boosted the studies of light to medium mass $N \sim Z$ nuclei [4] — previously, such investigations were mainly hampared by:

(i) the large number of different residual nuclei produced in the reactions (up to ~ 30),

* Presented at the XXXV Zakopane School of Physics "Trends in Nuclear Physics", Zakopane, Poland, September 5–13, 2000.

(ii) relatively large γ-ray energies (where detection efficiencies were low), and

(iii) considerable Doppler broadening caused by the large angle spread of recoils induced by charged-particle emission (see also, *e.g.*, Ref. [5]).

Here, recent advances in high-spin nuclear structure studies in the vicinity of ^{56}Ni shall be presented. ^{56}Ni is generally accepted to represent a doubly-magic spherical nucleus due to the shell gap at particle number 28, which separates the $1f_{7/2}$ shell from the so-called upper fp shell consisting of the $2p_{3/2}$, $1f_{5/2}$, and $2p_{1/2}$ orbits. The magicity reveals itself by a relatively large excitation energy of the first 2^+ state, and the rather irregular excitation scheme, which is shown on the left hand side of Fig. 1 [6]. It should be stressed that doubly-magic nuclei are important bench marks within the nuclidic chart, a point raised in several contributions to this school (see, *e.g.*, Ref. [7]), in particular related to the discussion of the regime of superheavy nuclei (see, *e.g.*, Ref. [**?**, 8]). The main issue is that these nuclei and their closeby neighbours serve as sources and act as constraints for the shell-model parameter sets, namely single-particle energies and two-body matrix-elements. A brief summary of the physics of the spherical minimum in $A \sim 60$ nuclei is given is Sec. 3.

Next to the spherical states the level scheme of ^{56}Ni contains also two regular sequences of γ-ray transitions, which begin at about 5 and 9 MeV excitation energy, respectively. They are interpreted as well-deformed rotational bands in the second minimum of the nuclear potential [6]. Such bands will be discussed more extensively in Sec. 4. The important point here is that their observation allows for a comparison of predictions of microscopic (large-scale) shell-model calculations *and* microscopic (*e.g.*, cranked Hartree-Fock) or macro-microscopic (*e.g.*, cranked Nilsson-Strutinsky) mean-field models, *i.e.*, it is possible to investigate the origin of nuclear deformation on a fundamental level.

One of the unexpected results mentioned in the beginning is the so-called prompt discrete particle emission, which connects high-spin states in the deformed second well with spherical states in the daughter nucleus. Up to now, this new exotic decay mode has only been found in nuclei near the $N = Z = 28$ doubly-magic isotope ^{56}Ni. Following the first case observed in ^{58}Cu [9] it was established in the excited rotational band in ^{56}Ni as well. It is illustrated on the right hand side of Fig. 1. Later-on, a 3.9(3)% α-decay branch was identified in the decay-out of a band in ^{58}Ni, while in Sec. 6 two new proton decays from bands in ^{59}Cu and new experimental results of combined γ-ray and particle spectroscopy in ^{58}Cu will be presented.

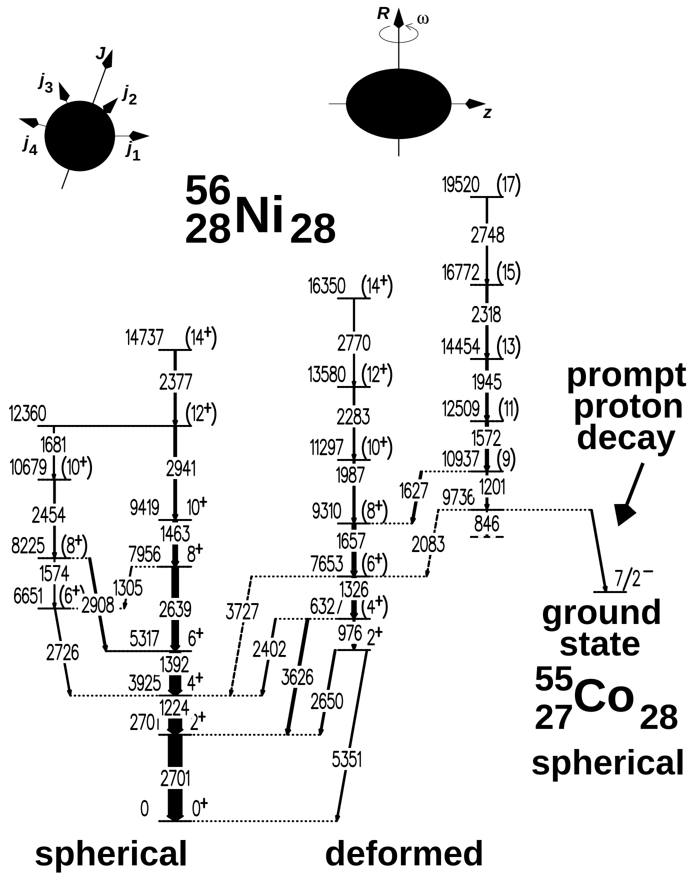

Fig. 1. Partial level scheme of ^{56}Ni.

2. Experiments

The nuclei in the mass $A \sim 60$ region were investigated in a series of experiments at GAMMASPHERE and EUROBALL. Table I summarizes the most recent ones, including the institutions involved. In all experiments 4π charged-particle detector arrays (MICROBALL [10] at GAMMASPHERE and ISIS [11] at EUROBALL) were coupled to the γ-detector arrays. Typical particle detection efficiencies amount to $\varepsilon_p \sim 80\%$ and $\varepsilon_\alpha \sim 65\%$ in the case of MICROBALL, following restrictive discrimination procedures (see, *e.g.*, Refs. [10, 12]). The respective numbers for ISIS turned out to be lower for the present EUROBALL experiment. For most of the experiments neutron detectors ($\varepsilon_n \sim 5$–10%) or dedicated neutron arrays ($\varepsilon_n \sim 30\%$) (NEUTRON-SHELL [13] at GAMMASPHERE and NEUTRONWALL [14] at EUROBALL) were used to identify evaporated neutrons, and thereby discriminating isotopes

TABLE I

Parameters of our recent experiments in the mass $A \sim 60$ region.

No.	Reaction	Beam energy	Label	Date	Target	Ancillary detectors[a]
1	^{32}S+^{28}Si	130 MeV	GSFMA73	9/99	thin	MB+NS
	(WashU, Lund, LBNL, ANL)					
2	^{36}Ar+^{28}Si	148 MeV	GSFMA42	12/98	thin	MB+SS+n
	(Lund, WashU, Cologne, UPenn, ORNL, ANL)					
3	^{24}Mg+^{40}Ca	96 MeV	EB98.02	9/98	backed	ISIS+NW
	(Lund, LNL, Cologne, TSL, Surrey, Warsaw, Bogota)					
4	^{28}Si+^{40}Ca	122 MeV	GSFMA66	7/99	thin	MB+BGO
	(LBNL, Lund, WashU, McMaster, Cologne, ANL)					

[a] MB: Microball [10]; NS: NeutronShell [13]; SS: Four ΔE–E Si-strip telescopes; n: 20 neutron detectors; Isis [11]; NW: NeutronWall [14]; BGO: full BGO information taken.

at or beyond the $N = Z$ line. The relatively low γ-ray multiplicities of the present experiments allow for a removal of the Heavimet absorbers in front of the BGO shields at Gammasphere [15]. This enables event-by-event γ-ray multiplicity and sum-energy measurements, which provides additional reaction channel selectivity [16]. Experiment 2 aimed at high-resolution particle spectroscopy. Therefore, the three most-forward rings of Microball (28 CsI-detector elements) were replaced by four ΔE–E Si-strip telescopes with a total of $4 \times 16 \times 16 = 1024$ pixels (see Sec. 6.3).

3. Spherical minimum

Figure 2 illustrates the shell structure for spherical and deformed nuclear shapes in the vicinity of ^{56}Ni. Different from $1f_{7/2}$ mid-shell nuclei (see Ref. [17] and references therein) unrestricted full fp shell-model calculations are not possible at present. For example, the shell-model study of ^{56}Ni [6], performed by Poves and co-workers, was 'limited' to six-particle six-hole $(6p - 6h)$ excitations across the shell gap at particle number 28.

Looking at the left hand side of Fig. 2 it is tempting to think that the full fp model space should be sufficient to describe the high-spin states in the ^{56}Ni region — there are several orbits available above the gap, and the high-j orbit $1g_{9/2}$ seems too far away. In fact, it is possible to describe the main features of the experimental decay schemes by simple shell-model calculations restricted to 2p-2h excitations [18]. Nevertheless, there are sequences in, *e.g.*, ^{54}Fe or ^{57}Ni, which are clearly outside the fp model space [18]. In ^{57}Ni such a sequence is located on top of a level at 3.7 MeV excitation energy, which was unambigously identified as representing the neutron $1g_{9/2}$ single-particle state by means of two linear polarization measurements [19]. This implies that a proper description of spherical shell-model states near ^{56}Ni needs to include both $1f_{7/2}$ holes *and* $1g_{9/2}$ particles. Such a model space is clearly beyond the scope of contemporary large-scale shell-model calculations with a full diagonalization of the Hamiltonian, but with quantum Monte-Carlo techniques the problem has already been tackled [20].

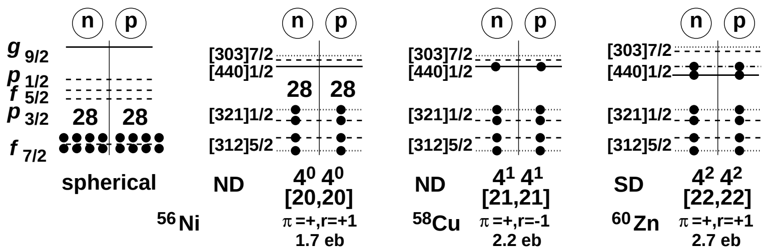

Fig. 2. Shell structure near ^{56}Ni.

4. Deformed minimum

Next to the spherical shell gap at particle number 28 there is also a gap of similar size for a prolate deformed ($\beta_2 \sim 0.4$) ^{56}Ni nucleus (*cf.* Fig. 2), which is due to a $4p$–$4h$ excitation — the [303]7/2 Nilsson orbit is emptied and the [321]1/2 orbit occupied for neutrons and protons. At the same time the $\mathcal{N} = 4$ high-j low-Ω [440]1/2 intruder orbit reaches the Fermi surface. It is readily occupied in the yrast deformed and superdeformed bands in ^{58}Cu [9] and ^{60}Zn [21], which may be called the 'doubly-magic deformed' (4^14^1) and 'doubly-magic superdeformed' (4^24^2) nuclei of the mass region, because large and very stable shell gaps appear for $N = Z = 29$ at $\beta_2 \sim 0.4$ and $N = Z = 30$ at $\beta_2 = 0.5$ in the rotating frame.

Figure 3 provides an overview of rotational bands currently known in the $A \sim 60$ region. Next to a number of straight $E2$ cascades, the first of which

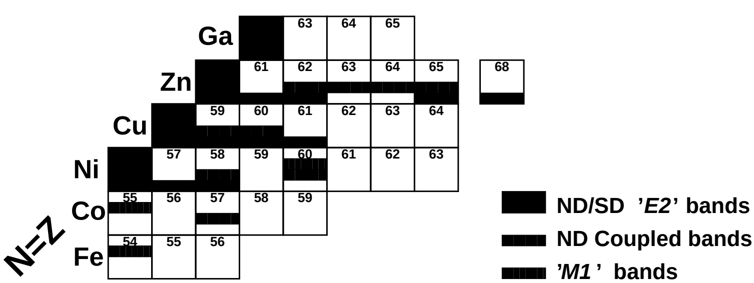

Fig. 3. Rotational bands in the mass $A \sim 60$ region (as of September 2000).

was discovered by Svensson *et al.* in ^{62}Zn [22], also coupled bands with more or less intense $\Delta I = 1$ cross over transitions were identified in the Ni, Cu, and Zn isotopes, which may arise from single nucleons in (relatively) high-K Nilsson orbits of the $1f_{7/2}$ shell. The first such rotational band *below* Ni was recently found in ^{57}Co [23]. It should be noted that different from other mass regimes almost all of the bands known are linked to the states in the spherical minimum, which fixes their excitation energies and allows for at least tentative spin and parity assignments. Some of the coupled bands have been observed up to terminating spins as well [24]. Comparisons of predictions of several microscopic and macro-microscopic models to the experimental observations have usually a very high level of agreement. Last but not least there are a few candidates for magnetic rotation in ^{54}Fe, ^{55}Co, and ^{60}Ni. They await, however, confirmation in terms of lifetime measurements. Such investigations are ongoing.

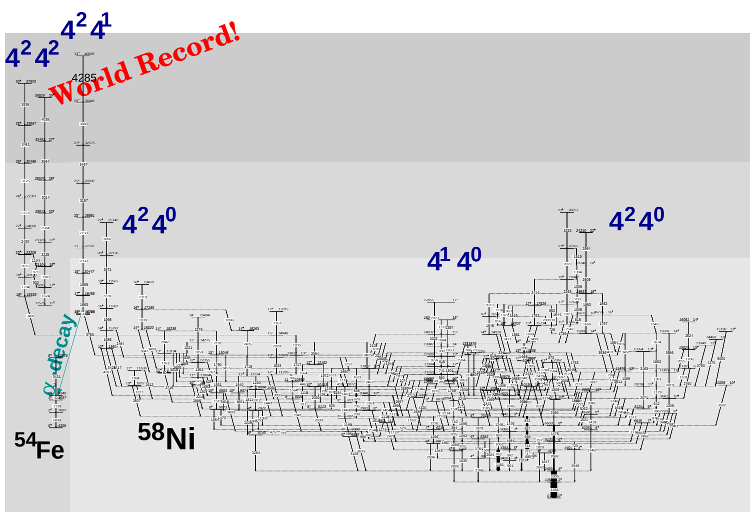

Fig. 4. Partial level scheme of ^{58}Ni.

The evolution of shapes in the mass region may be followed most beautifully in the case of ^{58}Ni [25]. Figure 4 provides an extensive (preliminary) excitation scheme of ^{58}Ni studied with three different reactions. From experiment 4 (*cf.* Table I) an extremely rich level scheme in the spherical minimum was established reaching states up to about 20 MeV excitation energy. ^{58}Ni represented the $2\alpha 2p$ channel, and was populated with a relative cross section of about 6%. The results from experiments 2 and 3 (and an earlier GAMMASPHERE experiment) allowed for an extension to 30 MeV excitation energy, and the level scheme becomes much more simple, since only rotational bands appear above 20 MeV. The relative cross section increases to some 30% for the $1\alpha 2p$ channel, which allows for extensive spectroscopy even for very weak transitions. Most importantly, an unprecedented discrete α decay from one of the bands could be established [26]. Last but not least, experiment 1 populated extremly high-spin states up to 40 MeV excitation energy in ^{58}Ni via $2p$ evaporation. The cross section becomes very small. In essence only the bands on the left hand side of Fig. 4 and their decay are observed. Finally, the topmost transition of 4285 keV in the $4^2 4^1$ band probably marks the current world record in terms of rotational frequency in high-spin nuclear structure.

5. $N = Z$ issues

5.1. $T = 0$ pairing

The fact that some of the nuclei of interest are $N = Z$ nuclei immediately raises the question whether some influence of isoscalar or isovector neutron-proton pairing or neutron-proton pair correlations are visible in the presumably clean configurations in the second minimum. The superdeformed band in ^{60}Zn reveals a band crossing at a rotational frequency of $\hbar\omega \approx$1.0 MeV [21], which can be explained in terms of a band crossing due to the simultaneous alignment of pairs of $g_{9/2}$ neutrons and protons. However, the expected proton alignment in $^{61}_{30}$Zn [27] and the neutron alignment in ^{59}Cu$_{30}$ [28], are not observed at this frequency. The expected alignments in the odd-A neighbours of ^{60}Zn are either absent, or they occur at considerably lower frequencies, which may be taken, along with other arguments [29], as a sign of neutron-proton pairing effects. However, the deformations of the three bands are rather different, and the subject is under discussion (see, *e.g.*, Ref. [30]).

5.2. Mirror nuclei

Another topic related to the $N = Z$ line is the study of mirror symmetry. Different from earlier studies of mirror nuclei in the $1f_{7/2}$ shell (see, *e.g.*, Ref. [31] and references therein) such investigations may nowadays invoke more detailed spectroscopic quantitites such as branching ratios, b, multipole mixing ratios, δ, or transition probabilities, $B(E2)$, to obtain limits for effective operators such as effective charges and effective g-factors. The idea is illustrated in Fig. 5 (see Ref. [32] for more details). The solid lines in parts (a) and (b) show the predicted ratios of the $B(E2; 27/2 \to 23/2^-)$ (a) and $B(E2; 17/2 \to 13/2^-)$ (b) values of the two $A = 51$ mirror nuclei $^{51}_{26}$Fe$_{25}$ and $^{51}_{25}$Mn$_{26}$, respectively, as a function of the effective proton charge e_p (the sum of effective proton and neutron charges is kept constant at 2.0). For a given shell-model parametrization a precise measurement of

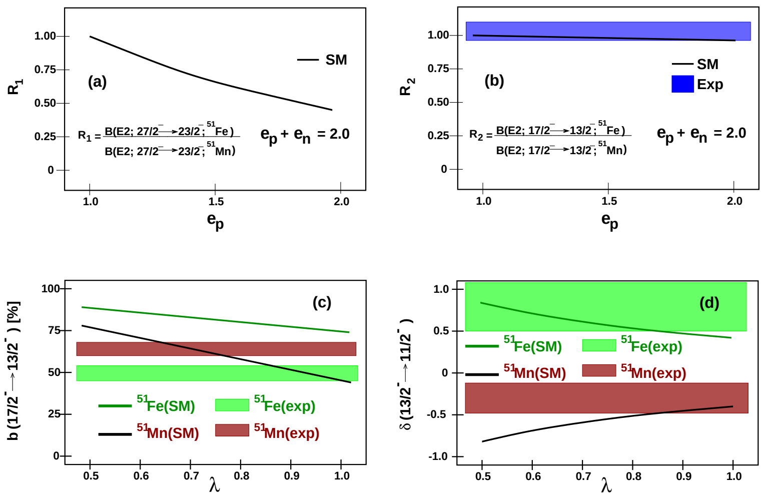

Fig. 5. Electromagnetic decay properties of $A = 51$ nuclei. See text for details.

the first ratio could clearly limit the effective charges, while the second ratio is rather insensitive to these parameters. Unfortunately, only for the latter we know the experimental values for both nuclei [33]. However, it is possible to use this weak dependence, since one can select a reasonable value for the effective proton charge ($e_p = 1.3$), and investigate how the branchings of the $17/2^- \to 13/2^-$ transitions depend on effective g-factors, $g_{\rm eff}$. This is shown in Fig. 5(c). λ denotes the fraction of the free g-factor. There is an agreement between the theoretical value and the experimental value for ^{51}Mn at $\lambda \approx 0.7$. There is no such agreement for ^{51}Fe, which can be associated with the problems in describing the decays of the $17/2^-$ states properly [32,33]. How the multipole mixing ratio $\delta(E2/M1)$ depends on $g_{\rm eff}$ is shown in Fig. 5(d). The shell-model calculations reproduce the opposite signs measured for $\delta(E2/M1)$ and $\lambda \approx 0.85$ would be consistent with both measured values.

6. Proton decays

6.1. Two prompt proton decays in ^{59}Cu

The isotope ^{59}Cu has only one neutron added to the $N = Z$ nuclide ^{58}Cu, in which the new exotic decay mode of prompt proton emission had been observed for the first time [9]. By looking at energy and spin relations between the excitation energies of rotational bands in ^{59}Cu and possible spherical daughter states in ^{58}Ni it becomes clear that ^{59}Cu is an excellent candidate to search for this new decay mode. In fact, greatly improved statistics for ^{59}Cu in experiment 4 (*cf.* Table I) as compared to earlier runs (see, *e.g.*, Ref. [28]) allowed for the discrimination of "two prompt proton decays from two different bands with two different intruder configurations with two different energies with two different branching ratios into two different spherical states of ^{58}Ni" [35].

TABLE II

Summary of prompt particle decays in the mass $A \sim 60$ region (as of September 2000).

Nuclide	Particle	Q-value (MeV)	Branching (%)	Spin difference	Reference
^{56}Ni	proton	2.57	49(14)	$(7/2^+)$	[6]
^{58}Ni	alpha	7.45	3.9(3)	(9^-)	[26]
^{58}Cu	proton	2.34	> 97	$(9/2)^+$	[9]
^{59}Cu	proton	1.92	~ 4	$9/2^+$	[35]
	proton	2.50	~ 16	$9/2^+$	[35]

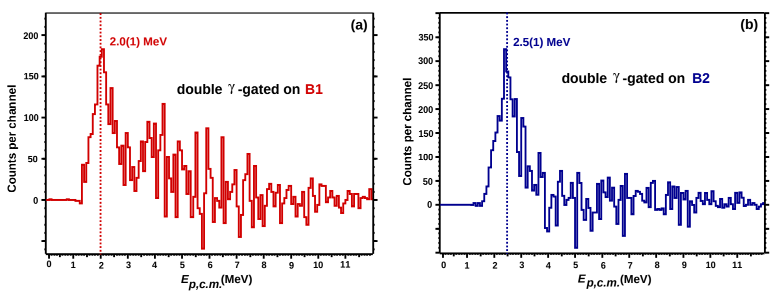

Fig. 6. Proton center-of-mass energy spectra for two prompt proton decays in ^{59}Cu. See Ref. [35] for more details.

Figure 6 shows proton center-of-mass energy spectra (*cf.* Sec. 6.3) in coincidence with the yrast superdeformed band $(4^2 4^1)$ [Fig. 6(a)] [28] and an excited rotational band $(4^1 4^1)$ in ^{59}Cu [Fig. 6(b)] [35]. The spectra are also subject to an overall $2\alpha 2p$ particle gate, since ^{59}Cu represents the $2\alpha 1p$ evaporation channel of the experiment, and the second proton of the gate shall be the decay proton. Only protons detected in the first four rings of MICROBALL are used to increment the spectra in Fig. 6 (*cf.* Ref. [12]), and the "background" of evaporation protons has been subtracted [35]. The peak energies of 2.0(1) and 2.5(1) MeV are in agreement with the Q-values between the superdeformed 11921 keV $25/2^+$ state in ^{59}Cu and the spherical 8^+ yrast state in ^{58}Ni, and the well-deformed 11984 keV $23/2^-$ level in ^{59}Cu and the 7^- yrast state in ^{58}Ni, respectively. The decay paths are fixed also due to γ-ray coincidences between transitions in the parent and daughter nucleus, and the branching ratios were determined to $\sim 4\%$ and $\sim 16\%$, respectively [35]. In both cases the decaying proton appears to be the single $1g_{9/2}$ proton in the band configuration. Table II summarizes the main quantities for the presently (September 2000) known prompt particle decays.

6.2. The lifetime of the proton-decaying state in ^{58}Cu

Experiment 3 was aiming mainly at electromagnetic decay properties of mass $A \sim 60$ nuclei. Applying the Doppler Shift Attenuation Method to levels in ^{58}Cu, lifetimes of individual states at the bottom of the rotational band could be determined [36]. The 830 keV line, which depopulates the 9745 keV state and feeds the proton-decaying level at 8915 keV, reveals both a stopped and a shifted component in its lineshape observed in the backward-angle CLUSTER section [*cf.* Fig. 7(a) and (e)]. Since the 3701 keV $9/2^+$ daughter state in ^{57}Ni has a lifetime in excess of two picoseconds, energy correlations between the 830 keV γ ray measured in the CLUSTER detectors and the 2.3 MeV proton peak [9] in the most forward detector elements of ISIS were studied. The result is shown in Fig. 7. The upper row shows spectra obtained from a channel-selected E_γ-$E_{p,\mathrm{lab}}$ matrix, while for the lower row a second γ ray corresponding to one of the transitions in the ^{58}Cu band had to be detected.

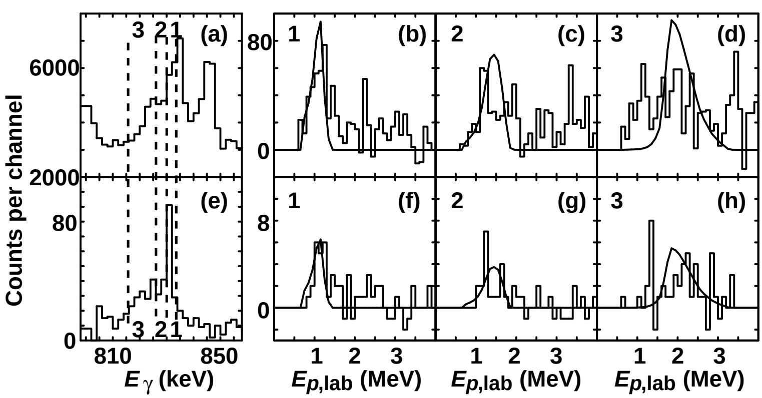

Fig. 7. Proton-γ energy correlations. See text for details.

Figures 7(a) and (e) present the total projections of the two matrices near the 830 keV line. Three regions are indicated, which correspond to stopped, slightly shifted, and shifted components of that transition. Figures 7(b)–(d) and 7(f)–(h) are the corresponding background-subtracted coincident proton-energy spectra. The solid lines are Monte-Carlo simulations [37] of the most forward ring of ISIS. The basic result is that the shifted component of the γ-ray is in essence in coincidence with a shifted component of the proton line (region 3), while the gate on the stopped component of the γ-ray brings back the stopped component of the proton peak (region 1). Hence, the lifetime of the particle decay out of the 8915 keV state is governed by the γ decay of the 9745 keV state, *i.e.*, considerably shorter than the previous upper limit of 3 ns [9].

6.3. Particle spectroscopy

A detailed study of the prompt particle decays is hampered by the relatively large widths of the peaks in the particle center-of-mass energy spectra (see Fig. 6). It turns out that the main contribution to the widths is not the intrinsic energy resolution of the CsI elements of MICROBALL, but the size of the solid angle. The center-of-mass energy is determined from the measured energy in the laboratory system and the kinetic energy of the particle at the time of emission resulting from the motion of the emitting system (recoil), according to

$$E_{\mathrm{CM}} = E_{\mathrm{lab}} + E_{\mathrm{kin}} - 2\sqrt{E_{\mathrm{lab}}E_{\mathrm{kin}}}\cos\Theta \qquad (1)$$

with Θ being the angle between the recoil direction and the detector. If one for a moment neglects the angle spread of the recoils after the evaporation process and plugs reasonable numbers for $E_{\mathrm{lab}} = 6.25$ MeV and $E_{\mathrm{kin}} = 1.25$ MeV into this equation for a detector element in ring 2 of MICROBALL ($\Theta = 21^\circ \pm 7^\circ$) one obtains center-of-mass energies which spread between $E_{\mathrm{CM}} = 2.08$ MeV ($\Theta = 14^\circ$) and 2.56 MeV ($\Theta = 28^\circ$), *i.e.*, almost 500 keV. To overcome this handicap we decided to replace the 28 most forward elements of MICROBALL with an array of four ΔE-E Si-strip telescopes providing some 800 active pixels instead (see, *e.g.*, Ref. [38] for details). This reduces the geometric opening angle to $\Delta\Theta \sim 2.5^\circ$ for a single pixel and the corresponding energy spread down to $\Delta E_{\mathrm{CM}} \sim 80$ keV. It is not reasonable to further tighten the angle coverage, because a beam spot of only 2 mm almost doubles the effective angle coverage of a pixel, *i.e.*, it will be diffcult to maintain this geometrical contribution to the energy resolution below some 150 keV throughout a presumed seven-day experiment.

The second (and in the case of experiment 2 largest) contribution to the peak width is the target thickness. A reaction can take place at the beginning or the end of the target, and it is impossible to determine the precise spot of an individual reaction on an event-by-event basis. Therefore, the kinematic energies for recoiling nuclei are different depending on their travel paths, hence energy loss, in the target foil. The particles of interest are emitted most likely *after* having passed through the remaining path of the thin target foil. The uncertainty in the *value* of the recoil velocity (the *direction* can be rather well determined from the energies and directions of evaporated particles) does lead to a kinematical contribution to the energy resolution of 200-250 keV for a target thickness of 0.5 $\mathrm{mg/cm^2}$.

Finally, the combination of intrinsic resolutions of ΔE and E strips ($\sim$ 50-60 keV each at 12 MeV) and the energy spread induced by $\sim 30\ \mathrm{mg/cm^2}$ thick Pb absorber foils, which are necessary to protect the array from direct heavy-ion hits, yields an intrinsic contribution of about 130 keV. The sum of the three contributions amounts to an expected resolution of about 300 keV for 2.0–2.5 MeV protons, and a preliminary analysis of actual data on ^{58}Cu yields some 350 keV, which should be compared to 700-800 keV obtained for the earlier experiments (*cf.* Sec. 6.1). It is hoped that a detailed and full analysis of experiment 2 will reveal possible weak decay branches from states known to particle decay, and to simplify the search for new cases. In addition, more detailed spectroscopic information such as angular distributions or correlations shall be investigated to, *e.g.*, determine the particle angular momentum directly.

7. Summary

The mass $A \sim 60$ region reveals many exciting aspects of nuclear structure: (i) shell-model states near a doubly-magic isotope; (ii) deformed and superdeformed rotational bands in the second minimum; (iii) issues related to the self-conjugate nature of some nuclides; (iv) the unprecedented exotic decay of several of the bands through discrete prompt particle emission in competition to conventional γ decay out mechanisms. The new experiments aiming at combined in-beam γ and particle spectroscopy are clearly challenging the present combinations of the 4π Ge-detector arrays and ancillary detector systems.

First of all, D.R. would like to thank the Organizing Committee for the invitation and kind hospitality during the school. We are grateful to those having contributed to the performance and successful running of the experiments mentioned in the text, namely A. Algora, R.A.E. Austin, D. Balamuth, R. Cardona, M.P. Carpenter, C. Chandler, R.J. Charity, R.M. Clark, M. Cromaz, G. de Angelis, M. Devlin, J. Eberth, P. Fallon, E. Farnea, A. Galindo-Uribarri, J. Garcés Narro, P. Hausladen, R.V.F. Janssens, T.L. Khoo, F. Kondev, T. Lauritsen, A.O. Macchiavelli, J. Nyberg, M. Palacz, Zs. Podolyák, W. Reviol, T. Rodinger, D. Seweryniak, L.G. Sobotka, T. Steinhardt, C.E. Svensson, O. Thelen, V. Tomov, and J.C. Waddington, as well as for the excellent support from the staff at the host laboratories in Argonne and Legnaro. This research was supported in part by the Swedish Natural Science Research Council, the U.S. Deparment of Energy [DE-FG05-88ER40406(WU)], and the European Community TMR/LSF Contract No. ERBFMGECT980110.

REFERENCES

[1] EUROBALL III, A European γ-ray Facility, Eds. J. Gerl and R.M. Lieder, GSI 1992.

[2] I.-Y. Lee, *Nucl. Phys.* **A520**, 641c (1990).

[3] GAMMASPHERE, The Beginning ... 1993-1997, Science Highlights booklet, Ed. M.A. Riley, (1998); `http://www-gam.lbl.gov`.

[4] Proceedings *Pingst 2000 – Selected Topics on $N = Z$ Nuclei*, June 2000, Lund, Sweden, eds. D. Rudolph and M. Hellström, KFS AB Lund, to be published.

[5] P. Bednarczyk *et al.*, *Acta Phys. Pol.* **32**, 747 (2001).

[6] D. Rudolph *et al.*, *Phys. Rev. Lett.* **82**, 3763 (1999).

[7] A. Covello *et al.*, *Acta Phys. Pol.* **32**, 000 (2001).

[8] I. Muntian, A. Sobiczewski, *Acta Phys. Pol.* **B32**, 629 (2001); I. Muntian, Z. Patyk, A. Sobiczewski, *Acta Phys. Pol.* **B32**, 691 (2001).

[9] D. Rudolph *et al.*, *Phys. Rev. Lett.* **80**, 3018 (1998).

[10] D.G. Sarantites *et al.*, *Nucl. Instrum. Meth.* **A381**, 418 (1996).

[11] E. Farnea *et al.*, *Nucl. Instrum. Meth.* **A400**, 87 (1997).

[12] D. Rudolph, in *The Nucleus: New Physics for the New Millenium*, January 1999, Faure, South Africa, Eds. F.D. Smit, R. Lindsay, and S. Förtsch, Kluwer Academic / Plenum Publishers, New York (1999), p. 397.

[13] D.G. Sarantites *et al.*, to be published.

[14] Ö. Skeppstedt *et al.*, *Nucl. Instrum. Meth.* **A421**, 531 (1999).

[15] M. Devlin *et al.*, *Nucl. Instrum. Meth.* **A383**, 506 (1996).

[16] C.E. Svensson *et al.*, *Nucl. Instrum. Meth.* **A396**, 228 (1997).

[17] D.R. Napoli *et al.*, *Acta Phys. Pol.* **B32**, 717 (2001).

[18] D. Rudolph *et al.*, *Eur. Phys. J.* **A4**, 115 (1999).

[19] D. Rudolph *et al.*, *Eur. Phys. J.* **A6**, 377 (1999); D. Rudolph, in: International Conference on Achievements and Perspectives in Nuclear Structure, July 1999, Crete, Greece, Eds. S. Åberg and C. Kalfas, *Phys. Scripta* **T88**, 21 (2000).

[20] T. Mizusaki, T. Otsuka, M. Honma, B.A. Brown, in: International Conference on Achievements and Perspectives in Nuclear Structure, July 1999, Crete, Greece, Eds. S. Åberg and C. Kalfas, *Phys. Scripta* **T88**, 107 (2000).

[21] C.E. Svensson *et al.*, *Phys. Rev. Lett.* **82**, 3400 (1999).

[22] C.E. Svensson *et al.*, *Phys. Rev. Lett.* **79**, 1233 (1997).

[23] W. Reviol *et al.*, in: Proceedings Nuclear Structure 2000, August 2000, East Lansing, U.S.A., to be published.

[24] C.E. Svensson *et al.*, *Phys. Rev. Lett.* **80**, 2558 (1998).

[25] D. Rudolph *et al.*, to be published.

[26] D. Rudolph *et al.*, *Phys. Rev. Lett*, in press.

[27] C.-H. Yu *et al.*, *Phys. Rev.* **C60**, 031305(R) (1999).

[28] C. Andreoiu *et al.*, *Phys. Rev.* **C62**, 051301(R) (2000).
[29] C.-H. Yu *et al.*, *Phys. Rev.* **C62**, 041301(R) (2000).
[30] A.V. Afanasjev, P. Ring, I. Ragnarsson, in [4], p. 183.
[31] M.A. Bentley *et al.*, in [4], p. 222.
[32] J. Ekman *et al.*, in [4], p. 232.
[33] J. Ekman *et al.*, *Eur. Phys. J.* **A9**, 13 (2000).
[34] M.A. Bentley *et al.*, *Phys. Rev.* **C62**, 051303(R) (2000).
[35] C. Andreoiu *et al.*, in [4], p. 21, and to be published.
[36] D. Rudolph *et al.*, submitted to *Phys. Rev.* **C63**, 021301(R) (2000).
[37] A. Gadea *et al.*, Annual Report 1996, Laboratori Nazionali di Legnaro, p. 118, 1997.
[38] MICROBALL Home Page, http://wunmr.wustl.edu/~dgs/mball, Section 7.